ELSEVIER

PII: S0309-1708(97)00004-3

Advances in Water Resources, Vol. 21 (1998) 351–362

0309-1708/98/$19.00+0.00

A numerical method for simulating non-Newtonian fluid flow and displacement in porous media

Yu-Shu Wu & Karsten Pruess

Earth Sciences Division, Ernest Orlando Lawrence Berkeley National Laboratory, Berkeley, CA 94720, USA

(Accepted 16 January 1997)

Flow and displacement of non-Newtonian fluids in porous media occurs in many subsurface systems, related to underground natural resource recovery and storage projects, as well as environmental remediation schemes. A thorough understanding of non-Newtonian fluid flow through porous media is of fundamental importance in these engineering applications. Considerable progress has been made in our understanding of single-phase porous flow behavior of non-Newtonian fluids through many quantitative and experimental studies over the past few decades. However, very little research can be found in the literature regarding multi-phase non-Newtonian fluid flow or numerical modeling approaches for such analyses.

For non-Newtonian fluid flow through porous media, the governing equations become nonlinear, even under single-phase flow conditions, because effective viscosity for the non-Newtonian fluid is a highly nonlinear function of the shear rate, or the pore velocity. The solution for such problems can in general only be obtained by numerical methods.

We have developed a three-dimensional, fully implicit, integral finite difference simulator for single- and multi-phase flow of non-Newtonian fluids in porous/fractured media. The methodology, architecture and numerical scheme of the model are based on a general multi-phase, multi-component fluid and heat flow simulator—TOUGH2. Several rheological models for power-law and Bingham non-Newtonian fluids have been incorporated into the model. In addition, the model predictions on single- and multi-phase flow of the power-law and Bingham fluids have been verified against the analytical solutions available for these problems, and in all the cases the numerical simulations are in good agreement with the analytical solutions. In this presentation, we will discuss the numerical scheme used in the treatment of non-Newtonian properties, and several benchmark problems for model verification.

In an effort to demonstrate the three-dimensional modeling capability of the model, a three-dimensional, two-phase flow example is also presented to examine the model results using laboratory and simulation results existing for the three-dimensional problem with Newtonian fluid flow.

Keywords: non-Newtonian fluid flow, reservoir simulation, power-law fluid, Bingham fluid, multi-phase flow.

1 INTRODUCTION

Flow and displacement of non-Newtonian fluids through porous media occurs in many subsurface systems and has found applications in underground natural resource recovery and storage projects, as well as environmental remediation schemes. Previous studies on the flow of fluids through porous media were limited for the most part to Newtonian fluids[1–3]. Since the 1950s, studies of non-Newtonian fluid flow through porous media have received a great deal of attention because of its important industrial applications, in petroleum industry, groundwater and environmental problems[4,5]. Considerable progress has been made in our understanding of single-phase porous flow behavior of non-Newtonian fluids through many quantitative and experimental studies in the past few

decades. However, little research can be found in the literature regarding multi-phase non-Newtonian fluid flow or numerical modeling approaches for such analyses.

Many studies on the flow of non-Newtonian fluids in porous media have been conducted in chemical engineering, rheology and petroleum engineering since the early 1960s. Because of the complexity of pore geometries in a porous medium, a macroscope continuum flux law has to be used to obtain meaningful insight into the physics of non-Newtonian flow in porous media. Some equivalent or apparent viscosities for non-Newtonian fluids are required in the Darcy equation. Therefore many experimental and theoretical investigations have been conducted to determine rheological models, or correlations of apparent viscosities with flow properties for a given non-Newtonian fluid as well as a given porous material. The viscosity of a non-Newtonian fluid depends upon the shear rate, or the velocity gradient. However, it is practically impossible to determine the distribution of the shear rate in a microscopic sense within a porous medium, and the rheological models developed in fluid mechanics for non-Newtonian fluids cannot be applied directly to porous media. As a result, many laboratory studies were undertaken in an attempt to relate the rheological properties of a non-Newtonian fluid to the pore flow velocity of the fluid or the imposed pressure drop in a real core or in a packed porous medium[4,6].

The subject of transient flow and displacement of non-Newtonian fluids in porous media is relatively new to many applications, starting from the late 1960s[7]. Pressure transient theory of flow of non-Newtonian power-law fluids in porous media was developed by Odeh and Yang[8] and Ikoku and Ramey[9]. Since then the new well test analysis techniques of non-Newtonian flow have been improved for interpreting pressure data observed during injectivity and falloff tests in reservoirs. The numerical modeling methods were also used for simulating power-law fluid flow by McDonald[10], Gencer and Ikoku[11], and Vongvuthipornchai and Raghavan[12,13].

Despite considerable advances over the past three decades in our understanding of single-phase porous medium flow behavior of non-Newtonian fluids through many quantitative and experimental studies, very little research has been conducted regarding multi-phase non-Newtonian fluid flow or numerical modeling approaches developed for such analyses. In some of our previous studies of non-Newtonian fluid flow, we developed a Buckley–Leverett[14]-type analytical solution for two-phase immiscible flow of non-Newtonian fluids in porous media[5,15,16], and applications of this solution have revealed many features of displacement of power-law and Bingham fluids. We also performed several numerical studies for simulating flow of single- and multi-phase non-Newtonian fluids in porous media[5,17,18].

This paper presents a three-dimensional, fully implicit, integral finite difference simulator developed for simulating single- and multi-phase flow of non-Newtonian fluids in porous/fractured media. The methodology, architecture and numerical scheme of the model are based on a general multi-phase, multi-component fluid and heat flow simulator, TOUGH2[19]. Several commonly used rheological models for power-law and Bingham non-Newtonian fluids have been incorporated into the model. In addition, the model predictions on single- and multi-phase flow of power-law and Bingham fluids have been verified against the analytical solutions available for these problems. In all the cases, the numerical simulations are in good agreement with the analytical solutions. A three-dimensional, five-spot, two-phase flow simulation example is also presented to examine the model results using laboratory and simulation results existing in the literature for Newtonian fluid displacement[20–22].

In this paper, we will present the numerical scheme used, the treatment of non-Newtonian properties and several benchmark problems for model verification.

2 MATHEMATICAL FORMULATION

2.1 Governing equations

The multiphase system is assumed to be isothermal and composed of three mass components, or three phases: air, water and a nonaqueous phase liquid (NAPL). The three components are assumed to be present only in their associated phases, i.e. mass transfer between phases for the components by equilibrium phase partitioning is ignored. Therefore, the present formulation is similar to 'dead oil' immiscible flow model. Two of the liquids, water and NAPL, can be considered as non-Newtonian fluids, while the gas phase is treated as a Newtonian fluid. In an isothermal system containing three mass components, three mass balance equations are needed to fully describe the system. The following summary of the governing flow equations follows Pruess[19,23,24,25] and Wu[5]. The balance equations for component or phase β (β = w, water; a, air; n, NAPL) are written in integral form for an arbitrary flow region V_ℓ with surface area Γ_ℓ as follows,

$$\frac{\mathrm{d}}{\mathrm{d}t}\int_{V_\ell} M_\beta \,\mathrm{d}V_n = \int_{\Gamma_\ell} \mathbf{F}_\beta \cdot \mathbf{n} \,\mathrm{d}\Gamma_n + \int_{V_\ell} q_\beta \,\mathrm{d}V_n \tag{1}$$

Here M_β is the mass of component β (β = w, a, n) per unit porous medium volume; F_β is the mass flux of component β into V_ℓ; $\mathbf{n}$ is the inward unit normal vector; and q_β is the rate of mass generation of component β per unit volume.

The mass accumulation terms for water, air and NAPL (β = w, a, n) in eqn (1) are defined as

$$M_\beta = \phi \sum_\beta S_\beta \rho_\beta \tag{2}$$

Here ϕ is the porosity; S_β is the saturation (pore volume fraction) occupied by phase β; and ρ_β is the β phase density.

The mass flux terms are given by a multiphase extension of Darcy"s law,

$$\mathbf{F}_\beta = -k\frac{k_{r\beta}\rho_\beta}{\mu_\beta}(\nabla P_\beta - \rho_\beta \mathbf{g}) \tag{3}$$

Here k is the absolute permeability; $k_{r\beta}$ is the relative permeability to phase β; μ_β is the β phase dynamic

viscosity, which for non-Newtonian fluids will be a generally non-linear function of flow rate; P_β is the fluid pressure in phase β; and $\mathbf{g}$ is the gravitational acceleration vector.

2.2 Supplementary relations

The mass transport governing eqn (1) needs to be supplemented with constitutive equations, which express all the parameters as functions of a set of primary thermodynamic variables of interest (P_β, S_β). The following relationships will be used to complete the statement of multiple phase flow of non-Newtonian and Newtonian fluids through porous media.

In addition to the three governing equations of eqn (1), there are supplementary equations given by

$$S_w + S_g + S_n = 1 \tag{4}$$

The aqueous and gas phase pressures are related by

$$P_w = P_g - P_{cgw}(S_w) \tag{5}$$

where P_{cgw} is the gas–water capillary pressure in a three-phase system, which is assumed to be a function of water saturation only. The NAPL phase pressure is related to the gas phase pressure by

$$P_n = P_g - P_{cgn}(S_w, S_n) \tag{6}$$

where P_{cgn} is the gas–NAPL capillary pressure in a three-phase system, which is a function of two phase saturations. For most geologic materials, the wettability order is (1) the aqueous phase, (2) the NAPL phase, and (3) the gas phase. The gas–water capillary pressure is usually stronger (more negative) than the gas–NAPL capillary pressure. The NAPL–water capillary pressure, in a three phase system, is

$$P_{cnw} = P_{cgw} - P_{cgn} = (P_n - P_w) \tag{7}$$

The relative permeabilities are assumed to be functions of fluid saturations only and not to be affected by non-Newtonian behavior, described by

$$k_{rw} = k_{rw}(S_w) \tag{8}$$

$$k_{rn} = k_{rn}(S_w, S_g) \tag{9}$$

$$k_{rg} = k_{rg}(S_g) \tag{10}$$

Here, the second liquid phase, NAPL, is assumed to be the intermediate wetting phase; its relative permeability depends on both wetting and nonwetting phase saturations.

Equations of state of the densities for Newtonian and non-Newtonian fluids are

$$\rho_\beta = \rho_\beta(P_\beta) \tag{11}$$

as functions of the individual phase pressures. For the gas phase, the ideal gas law is used.

Viscosities for Newtonian fluids are treated as constants, and for a non-Newtonian fluid, phase (β = n or w), the apparent viscosity may be expressed as a function of saturation and potential gradient[5]:

$$\mu_\beta = \mu_\beta(S_\beta, \nabla\Phi_\beta) \tag{12}$$

where $\nabla\Phi_\beta = \nabla P_\beta - \rho_\beta \mathbf{g}$.

2.3 Numerical discretization

The numerical technique presented in this work is the 'integral finite difference' method[25,26]. The numerical scheme implementation is based on the 'MULKOM/TOUGH2' family of multi-phase, multi-component codes[17,19,23]. The mass balance equations for each phase are expressed in terms of the integral finite difference equations, which are fully implicit to provide stability and time-step tolerance in highly nonlinear problems. Thermodynamic properties are represented by averages over explicitly defined finite subdomains, while fluxes of mass across surface segments are evaluated by finite difference approximations. All mass balance difference equations are solved simultaneously, using the Newton–Raphson iteration procedure.

The capillary pressures and relative permeabilities are treated as functions of saturation, and can be specified differently for different flow regions. The rheological properties for non-Newtonian viscosity require special treatments and depend on the rheological models used. Several common viscosity functions have been implemented in the code, such as the power-law and Bingham models.

The continuum expression [eqn (1)] is discretized in space using the 'integral finite difference' scheme, resulting in a set of first-order ordinary differential equations in time for element (grid block) ℓ,

$$\frac{dM_{\beta\ell}}{dt} = \frac{1}{V_\ell}\sum\nolimits_m A_{\ell m} F_{\beta,\ell m} + q_{\beta,\ell} \tag{13}$$

Here $F_{\beta,\ell m}$ is the average value of the (inward) normal component of mass flux over the surface segment $A_{\ell m}$ between volume elements V_ℓ and V_m. It is expressed in terms of averages over parameters for elements V_ℓ and V_m:

$$F_{\beta,\ell m} = -k_{\ell m}\left[\frac{k_{r\beta}\rho_\beta}{\mu_\beta}\right]_{\ell m}\left[\frac{P_{\beta,\ell} - P_{\beta,m}}{D_{\ell m}} - \rho_{\beta,\ell m} g_{\ell m}\right] \tag{14}$$

where the subscripts (ℓm) denote a suitable averaging between neighboring grid blocks (interpolation, harmonic weighting, upstream weighting); $D_{\ell m}$ is the distance between the nodal points ℓ and m; and $g_{\ell m}$ is the component of gravitational acceleration in the direction from m to ℓ. Time is discretized as a first-order difference, and the flux and sink and source terms on the right-hand side of eqn (13) are evaluated at the new time level, $t^{k+1} = t^k + \Delta t$, to obtain the numerical stability needed for an efficient calculation of multi-phase flow. This treatment of flux terms is known as 'fully implicit', because the fluxes are expressed in terms of the unknown thermodynamic parameters at time level t^{k+1}, so that these unknowns are only implicitly defined in the resulting equations. The time discretization

results in the following set of coupled nonlinear, algebraic equations:

$$R_{\beta,\ell}^{k+1} = M_{\beta,\ell}^{k+1} - M_{\beta,\ell}^{k} - \frac{\Delta t}{V_\ell}\left\{\sum_m A_{\ell m} F_{\beta,\ell m}^{k+1} + V_\ell (q_{\beta,\ell})^{k+1}\right\} = 0 \quad (15)$$

where we have introduced residual R to denote the difference between accumulation and flow terms.

For each volume element (grid block) V_ℓ there are three equations for the primary thermodynamic variables, P_g, S_n and S_g. For a flow system which is discretized into N grid blocks, eqn (15) represents a set of $3N$ coupled nonlinear, discretized algebraic equations. The unknowns are the $3N$ independent primary variables x_i ($i = 1, 2, 3, \ldots, 3N$) which completely define the state of the flow system at time level t^{k+1}. These equations are solved by Newton–Raphson iteration, which is implemented as follows. An iteration index p is introduced and the residuals at iteration level $p + 1$ are expanded in terms of the primary variables $x_{i,p}$ at iteration level p. Retaining only terms up to the first order, a set of $3N$ linear equations for the increments $(x_{i,p+1} - x_{i,p})$ is obtained:

$$-\sum_i \left.\frac{\partial R_{\beta,\ell}^{k+1}}{\partial x_i}\right|_p (x_{i,p+1} - x_{i,p}) = R_{\beta,\ell}^{k+1}(x_{i,p}) \quad (16)$$

All terms in the Jacobian matrix are evaluated by numerical differentiation and eqn (16) is solved with direct methods[27] or iteratively by means of preconditioned conjugate gradient solvers[28]. Iteration is continued until the residuals R_ℓ^{k+1} are reduced below a preset convergence tolerance, usually taken as $10^{-5} \times M_\ell^\kappa$.

3 TREATMENT OF NON-NEWTONIAN BEHAVIOR

The apparent viscosity functions for non-Newtonian fluids in porous media depend on the pore velocity, or the potential gradient, in a complex way[4]. The rheological correlations for different non-Newtonian fluids are quite different. Therefore, it is impossible to develop a general numerical scheme that can be universally applied to all non-Newtonian fluids. Instead, special treatment for a particular fluid of interest has to be worked out. Typical relationships of shear stress and shear rate for commonly encountered non-Newtonian fluids in porous media are shown in Fig. 1. For some most often used non-Newtonian fluids, such as the power-law and Bingham plastic fluids, the numerical treatment will be discussed here.

3.1 Power-law fluid

The power-law model[29] is the most widely used in describing the rheological property of shear-thinning fluids, such as polymer and foam solutions, in porous flow. Its multiphase

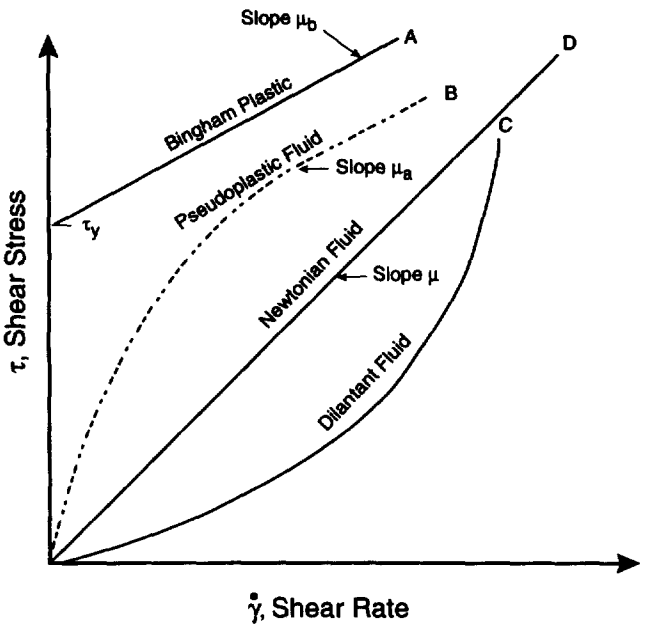

Fig. 1. Typical shear stress and shear rate relationships for non-Newtonian fluids.

extension[15]

$$\mu_{nn} = \mu_{eff}\left(\frac{k k_{rnn}(|\nabla\Phi|)}{\mu_{eff}}\right)^{\frac{n-1}{n}} \quad (17)$$

where subscript nn denotes a non-Newtonian fluid; n is the power-law index; $\nabla\Phi$ is flow potential gradient; and μ_{eff} is defined as

$$\mu_{eff} = \frac{H}{12}\left(9 + \frac{3}{n}\right)^n [150 k k_{rnn\phi}(S_{nn} - S_{nnir})]^{(1-n)/2} \quad (18)$$

where H is a consistence parameter; S_{nn} is the non-Newtonian, power-law fluid saturation, and S_{nnir} is irreducible saturation of the non-Newtonian phase. The two power-law parameters, n and H, are normally obtained from laboratory measurement and fitting data.

The power index, n, ranges between 0 and 1 for a shear thinning fluid, and the viscosity from eqn (17) becomes infinite as the flow potential gradient tends to zero. Therefore, direct use of eqn (17) in the calculation will cause numerical difficulties. Instead, a linear interpolation scheme is used when the potential gradient is very small. As shown in Fig. 2, the viscosity for a small value of potential gradient is calculated by

$$\mu_{nn} = \mu_1 + \frac{\mu_1 - \mu_2}{\delta_1 - \delta_2}(|\nabla\Phi| - \delta_1) \quad (19)$$

for $|\nabla\Phi| \le \delta_1$, where the two interpolation parameters are δ_1 ($\sim 10\ \text{Pa m}^{-1}$) and δ_2 ($\delta_1 - \delta_2 = 10^{-7}\ \text{Pa m}^{-1}$); and the values for μ_1 and μ_2 may be taken as (see Fig. 2),

$$\mu_j = \mu_{eff}\left(\frac{k}{\mu_{eff}}\delta_j\right)^{(n-1)/n} \quad (j = 1, 2) \quad (20)$$

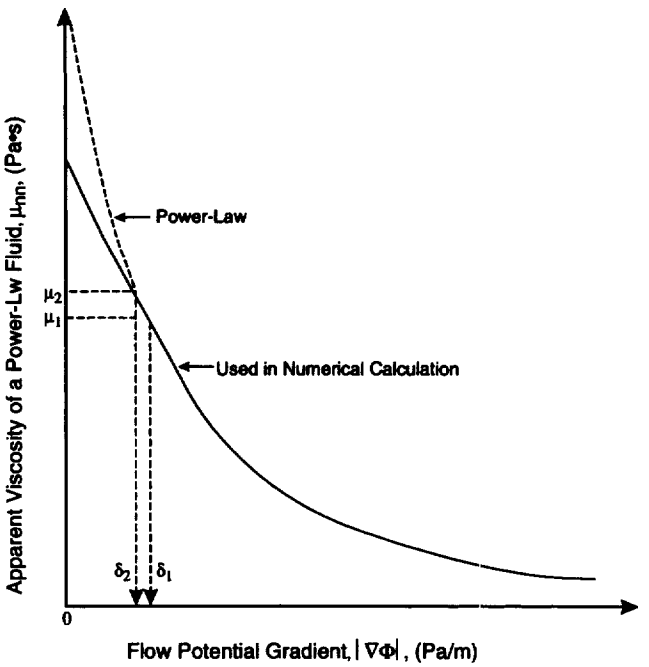

Fig. 2. Schematic of linear interpolation of viscoties of power-law fluids with small flow potential gradients.

3.2 Bingham fluid

Instead of introducing an apparent viscosity for Bingham fluids, the following effective potential gradient approach has been proven to be more efficient numerically. Using the effective potential gradient as illustrated by Fig. 3, Darcy's law of Bingham flow[16] is described by

$$\mathbf{u} = -\frac{kk_{rnm}}{\mu_b}\nabla\Phi_e \tag{21}$$

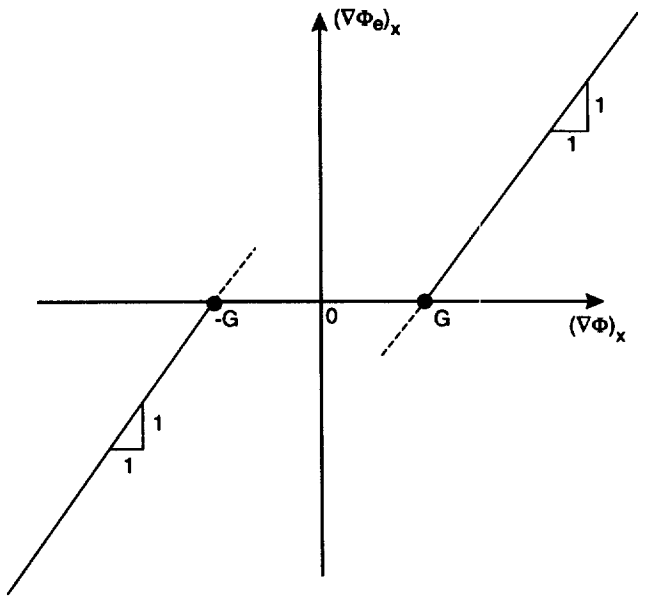

Fig. 3. Effective potential gradient for Bingham fluids, dashed linear extension for numerical calculation of derivatives.

where μ_b is the Bingham plastic viscosity coefficient and $\nabla\Phi_e$ is the effective potential gradient whose scalar component in the x-direction, flow direction, is defined as

$$(\nabla\Phi_e)_x = (\nabla\Phi)_x - G, \quad \text{if } (\nabla\Phi)_x > G$$
$$(\nabla\Phi_e)_x = (\nabla\Phi)_x + G, \quad \text{if } (\nabla\Phi)_x < -G$$
$$(\nabla\Phi_e)_x = 0, \quad \text{if } G \geq (\nabla\Phi) \geq -G$$

where G is the minimum potential gradient of Bingham fluids.

4 VERIFICATION AND SIMULATION SAMPLES

Four examples are given in this section to provide verification of the model numerical schemes. The samples problems includes: (1) one-dimensional displacement of a Newtonian fluid by a power-law, non-Newtonian fluid; (2) single-phase Bingham transient flow; (3) one-dimensional displacement of a Bingham fluid by a Newtonian fluid; and (4) a three-dimensional, five-spot, two-phase flow simulation example for which laboratory and simulation results are known in the literature for Newtonian fluid displacement[20–22]. For the first three problems, analytical solutions are available for model benchmarking. For the fourth, three-dimensional flow problem, the existing laboratory and numerical simulation results are used to check the simulations of the proposed model, applied to a special case of Newtonian flow. In addition a three-dimensional Bingham oil displacement is demonstrated by the problem.

4.1 Displacement of a Newtonian fluid by a power-law fluid

This example of interest is a one-dimensional immiscible flow problem of two incompressible fluids, one Newtonian and one non-Newtonian fluid, in a semi-infinite, horizontal, homogeneous and isotropic porous medium with a unit cross-sectional area. Capillary effects are assumed to be negligible. Under such conditions, an analytical solution is available through extension of the Buckley–Leverett method[15]. The problem is that a power-law fluid injected as a displacing agent to drive an initially saturated Newtonian liquid in a porous medium.

In order to reduce the effects of discretization in a finite system, very fine mesh spacing (Δx = 0.0125 m) was chosen for the first 240 elements, and then the spacing was increased by a factor of 1.5 for the 290th element. The properties of rock and fluids are given in Table 1, and a comparison of the saturation profiles from the numerical and analytical solution after 10 h of non-Newtonian fluid injection is shown in Fig. 4. The figure shows that the numerical results are in excellent agreement with the analytical solution, although some smearing occurs at the sharp front as normally seen for a Buckley–Leverett problem.

Table 1. Parameters for power-law fluid displacement

Porosity	$\phi = 0.20$
Permeability	$k = 1$ Darcy
Injection rate	$q = 0.8233 \times 10^{-5}\ m^3\ s^{-1}$
Injection time	$t = 10$ h
Displaced phase viscosity	$\mu_{ne} = 5$ cP
Irreducible Newtonian saturation	$S_{neir} = 0.2$
Irreducible non-Newtonian saturation	$S_{nn} = 0.0$
Power-law index	$n = 0.5$
Power-law coefficient	$H = 0.01\ Pa{\cdot}s^n$
Relative permeability to non-Newtonian phase	$k_{rnn} = 1.17\ (S_{nn})^2$
Relative permeability to Newtonian phase	$k_{rne} = 0.75(1 - 1.25S_{nn})^2$

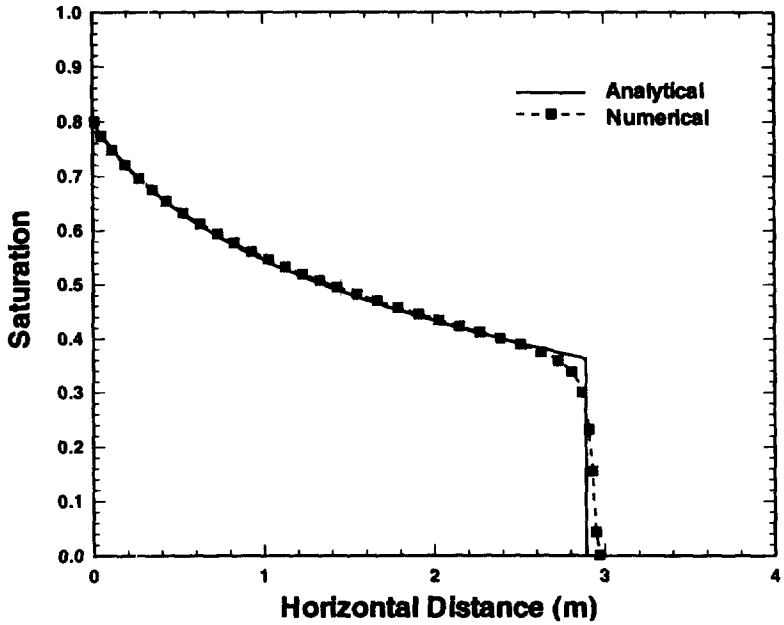

Fig. 4. Comparison of the power-law fluid saturation profiles from the numerical and analytical solutions at $t = 10$ h.

4.2 Transient radial flow of single-phase Bingham fluid

This is a one-dimensional transient radial flow problem of Bingham fluid, and an analytical solution is available[16] for this comparison study. The problem concerns a pumping test of a fully penetrating well at an infinite, homogeneous and horizontal reservoir with constant thickness. The reservoir is fully saturated with single-phase Bingham liquid, such as heavy oil. The pumping starts at time = 0 with constant mass pumping rate. The fluid and formation parameters used in this test are listed in Table 2.

Table 2. Parameters for single-phase Bingham fluid flow

Initial porosity	$\phi_i = 0.20$
Initial fluid density	$\rho_i = 975.9\ kg\ m^{-3}$
Initial pressure	$P_i = 10^7$ Pa
Mass pumping rate	$q_m = 1\ kg\ s^{-1}$
Bingham coefficient	$\mu_b = 5 \times 10^{-3}$ Pa·s
Minimum pressure gradient	$G = 1000\ Pa\ m^{-1}$
Fluid compressibility	$C_f = 4.557 \times 10^{-10}\ Pa^{-1}$
Formation thickness	$h = 1$ m
Rock compressibility	$C_r = 2.644 \times 10^{-9}\ Pa^{-1}$
Permeability	$k = 1$ Darcy
Wellbore radius	$r_w = 0.1$ m

Fig. 5 indicates that there exists excellent agreement between the two solution for the entire transient period. The pressure profiles along radial distance at $t = 1000$ s, predicted by the two methods, are compared in Fig. 6. The match of the numerical results with the analytical solution has been found to be excellent from early to later times at any radial distance.

4.3 Displacement of a Bingham fluid by a Newtonian fluid

This is another one-dimensional immiscible displacement problem, in which a Bingham liquid is displaced by a Newtonian fluid, similar to the case of heavy oil production by water flooding in petroleum industry. The problem description is similar to the power-law fluid displacement problem, and we also use the same analytical solution to examine the numerical simulation results. The one-dimensional rock column is initially saturated by a Bingham

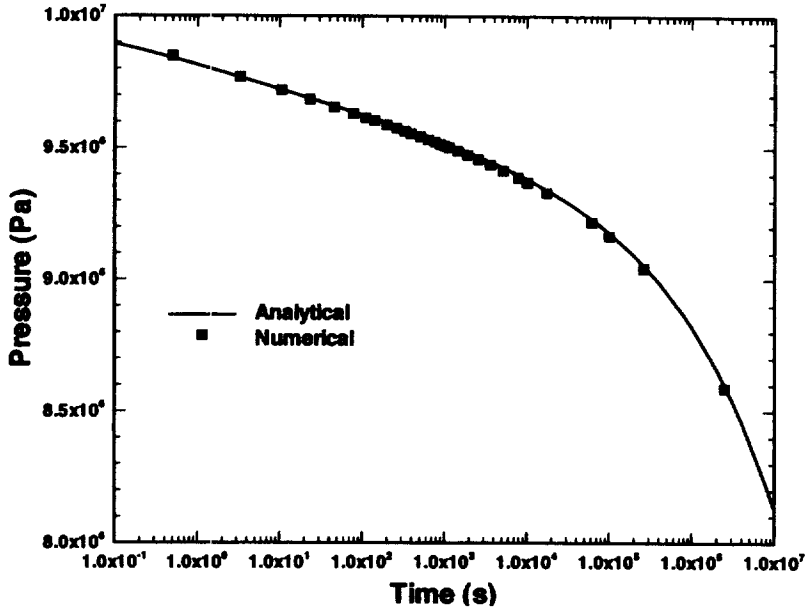

Fig. 5. Comparison of the wellbore pressures for the numerical and analytical solutions during pumping of a Bingham fluid.

fluid only, and then a Newtonian liquid (water) is injected at the inlet as a displacing agent to drive the Bingham liquid.

The properties of rock and fluids are given in Table 3, and a comparison of the saturation profiles from the numerical and analytical solutions after 1 day of water injection is shown in Fig. 7. Fig. 7 indicates that the numerical results are in good agreement with the analytical solution, although some small smearing at the sharp saturation front exists.

4.4 Three-dimensional, five-spot, two-phase problem

This example is a well-known three-dimensional flow problem, because the laboratory results are available[20], and it has been used in the literature for benchmarking of reservoir simulators[21,22]. The problem concerns oil recovery from a five-spot well pattern with the formation saturated with oil (70%) and water (30%) initially. The computational domain consists of a one-quarter five spot, and the dimensions are shown in Fig. 8, with a constant-rate injection well and a constant-rate pumping well at the diagonal corners, respectively.

The fluid and formation properties are summarized in Table 4, and the relative permeability and capillary pressure data are given in Table 5. A three-dimensional $10 \times 10 \times 5$ brick grid is used for this problem, with $\Delta x = \Delta y = 14.22$ m and $\Delta z = 1.22$ m. the formation is treated as homogeneous

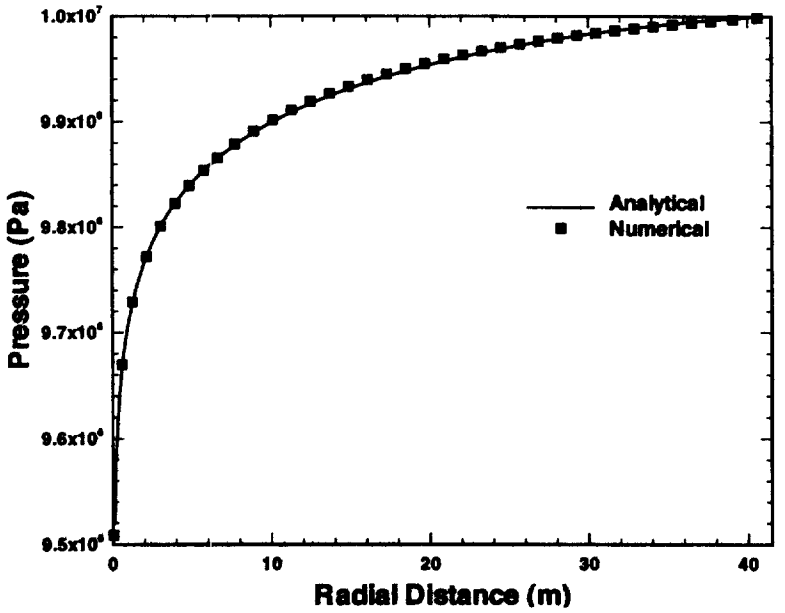

Fig. 6. Comparison of the pressure profiles from the numerical and analytical solutions at $t = 1000$ s during pumping of a Bingham fluid.

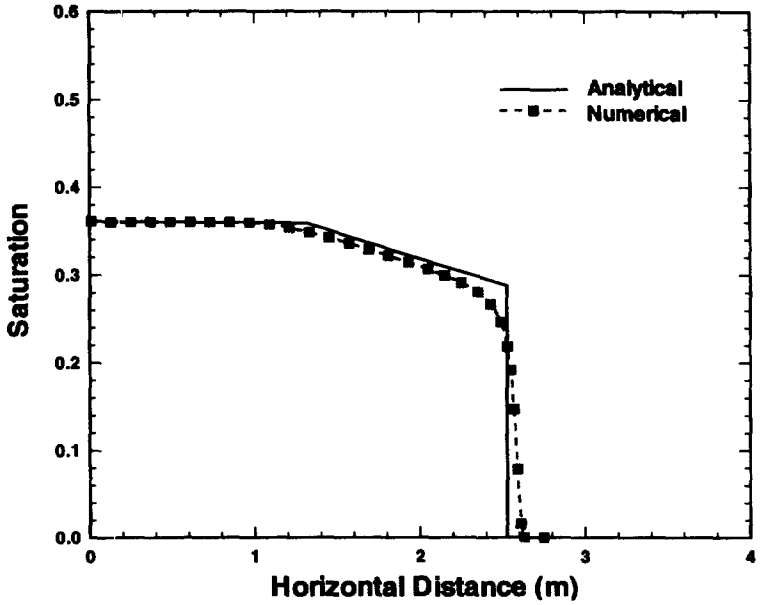

Fig. 7. Comparison of the water saturation profiles from the numerical and analytical solutions at $t = 1$ day of Bingham fluid displacement.

and the wells are fully penetrating. Both pumping and injection wells are treated fully implicitly in the code using the no back flow, potential allocation method[30].

Even though the flow domain for this problem is regular and horizontal, the flow is actually three-dimensional because of the gravity effects between oil and water phases. Water tends to flow downwards when flowing towards the pumping well, while oil tends to float to the top by the gravity forces during moving. The three-dimensional flow is also contributed by the nonuniform distributions of the injected and pumped fluxes along the wellbores.

There are two simulations conducted for this problem. The first simulation is treated oil as a Newtonian fluid, a special case of non-Newtonian fluids, and water is always a Newtonian fluid. The second simulation considers the oil as a heavy oil, or a Bingham fluid with the Bingham coefficient equal to the oil viscosity and the minimum pressure gradient $G = 10\,000$ Pa. Otherwise, the operation conditions and the simulation parameters are the same for the two runs. The experimental data and the simulated results obtained from the present and previous models are compared in Fig. 9. Fig. 9 shows that the cumulative oil recovery curves are similar. The present model for both Newtonian oil and non-Newtonian oil cases predicts slightly higher oil recovery over the range 0.3–0.8 pore volumes (PV) of water injection. The discrepancy may be due to the different rock characteristic curves used in the present and previous models[22]. Fig. 9 indicates that the 'heavy oil' recovery rate

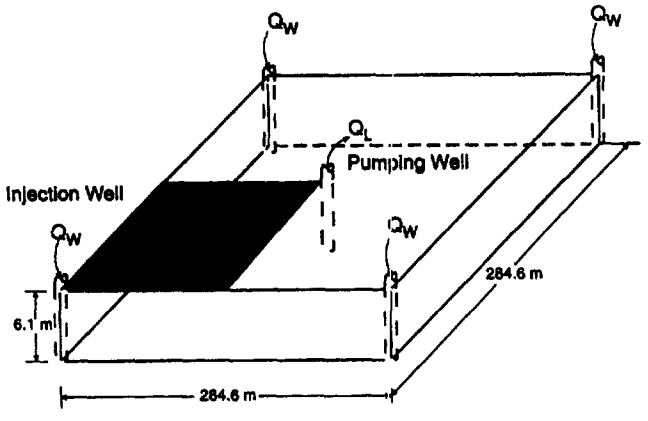

Fig. 8. Domain for the two-phase five-spot problem.

Table 3. Parameters for Bingham fluid displacement

Porosity	$\phi = 0.20$
Water density	$\rho_w = 1000\ \text{kg m}^{-3}$
Bingham fluid density	$\rho_{nn} = 900\ \text{kg m}^{-3}$
Water phase viscosity	$\mu_w = 1 \times 10^{-3}$ Pa·s
Bingham coefficient	$\mu_b = 2 \times 10^{-3}$ Pa·s
Minimum pressure gradient	$G = 10\,000\ \text{Pa m}^{-1}$
Permeability	$k = 1$ Darcy
Injection rate	$q = 2.0 \times 10^{-6}\ \text{m}^3\ \text{s}^{-1}$
Injection time	$t = 1$ day
Irreducible water saturation	$S_{wir} = 0.0$
Irreducible non-Newtonian saturation	$S_{nnir} = 0.2$
Relative permeability to Bingham fluid	$k_{rnn} = (1 - 1.25S_w)^2$
Relative permeability to water phase	$k_{rw} = 1.56(S_w)^2$

Table 4. Parameters for three-dimensional, five-spot, two-phase flow from the experiment reported by Gaucher and Lindley[20]

Porosity	$\phi = 0.20$
Water density	$\rho_w = 1000\ \text{kg m}^{-3}$
Oil density	$\rho_o = 800\ \text{kg m}^{-3}$
Water injection rate	$Q_w = 1.93 \times 10^{-5}\ \text{m}^3\ \text{s}^{-1}$
Total liquid pumping rate	$Q_L = 1.93 \times 10^{-5}\ \text{m}^3\ \text{s}^{-1}$
Water viscosity	$\mu_w = 0.5 \times 10^{-3}$ Pa·s
Bingham coefficient or oil viscosity	$\mu_b = 2.17 \times 10^{-3}$ Pa·s
Minimum pressure gradient	$G = 10\,000\ \text{Pa m}^{-1}$
Residual oil saturation	$S_{or} = 0.067$
Residual water saturation	$S_{wr} = 0.3$
Initial oil saturation	$S_o = 0.7$

Table 5. Relative permeability and capillary pressure data used for three-dimensional, five-spot, two-phase flow, estimated by Wu *et al.*[22]

S_w	k_{rw}	k_{ro}	P_c (Pa)
0.30000	0.00000	0.81250	0.4434×10^5
0.33164	0.00000	0.75002	0.3810×10^5
0.36328	0.00000	0.68935	0.3295×10^5
0.39492	0.00000	0.63055	0.2863×10^5
0.42656	0.00000	0.57365	0.2495×10^5
0.45820	0.00001	0.51870	0.2177×10^5
0.48984	0.00005	0.46578	0.1901×10^5
0.52148	0.00016	0.41492	0.1658×10^5
0.55312	0.00046	0.36622	0.1443×10^5
0.58476	0.00115	0.31973	0.1251×10^5
0.61640	0.00261	0.27556	0.1079×10^5
0.64804	0.00547	0.23379	0.9237×10^4
0.67968	0.01073	0.19455	0.7828×10^4
0.71132	0.01996	0.15797	0.6545×10^4
0.74296	0.03545	0.12420	0.5371×10^4
0.77460	0.06051	0.09346	0.4293×10^4
0.80624	0.09979	0.06598	0.3300×10^4
0.83788	0.15963	0.04212	0.2381×10^4
0.86952	0.24860	0.02238	0.1530×10^4
0.90116	0.37799	0.00759	0.7380×10^3
0.93280	0.56250	0.00000	0.0000×10^0

Table 6. Summary of computational performance for the sample problems

Problem	Number of elements	Time steps	Maximum time step size (s)	Simulation time (s)	CPU time (s)	Solver
4.1	240	586	64	3.6×10^4	567	Direct
4.2	401	300	Unlimited	1.5×10^{11}	432	Direct
4.3	326	469	227	8.64×10^4	444	Direct
4.4a Newtonian oil	500	76	8.64×10^8	3.16×10^9	479	Iterative
4.4b Bingham oil	500	74	8.64×10^8	3.16×10^9	490	Iterative

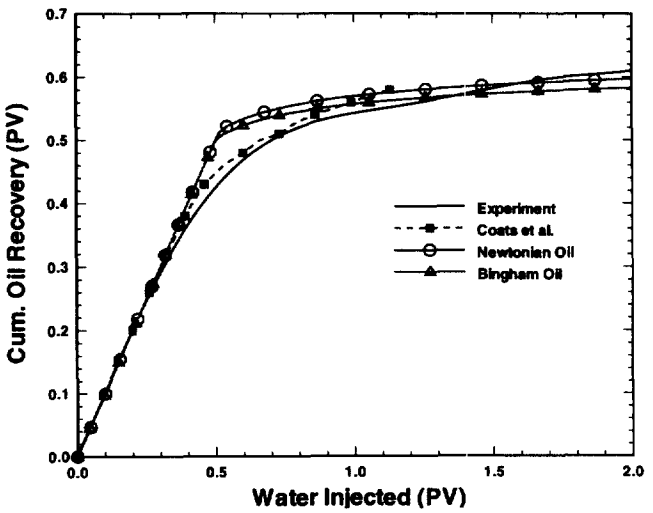

Fig. 9. Cumulative oil recovery and comparison for Newtonian and Bingham oil displacement for the two-phase five-spot problem.

is 2–3% lower than that for Newtonian oil after the early injection of 0.5 pore volumes because of the high flow resistance of Bingham flow behavior.

Figs 10 and 11 show the three-dimensional plots of oil saturations at 20 years for Newtonian and Bingham oils, respectively. A comparison of the two oil saturation distributions on the two figures indicates a clear difference between the two scenarios. First, the lower (green) oil saturation or water front is very close to the pumping well, and almost breakthrough on Fig. 11 for the Bingham oil case. For the Newtonian oil, however, Fig. 10 shows the water front still has a certain distance to the pumping well. Primarily along the left front boundary surface of the five-spot domain, the oil is still intact on Fig. 11, but water has already reached the surface near the pumping well for the case of Bingham oil, as shown in Fig. 11. Second, the curvatures of saturation contours on the top surface of the domain, along the diagonal direction from injection to pumping wells, indicate that there is more dominant diagonal water flow for the Bingham oil than for Newtonian oil. In addition, more oil or relative high oil saturation is left

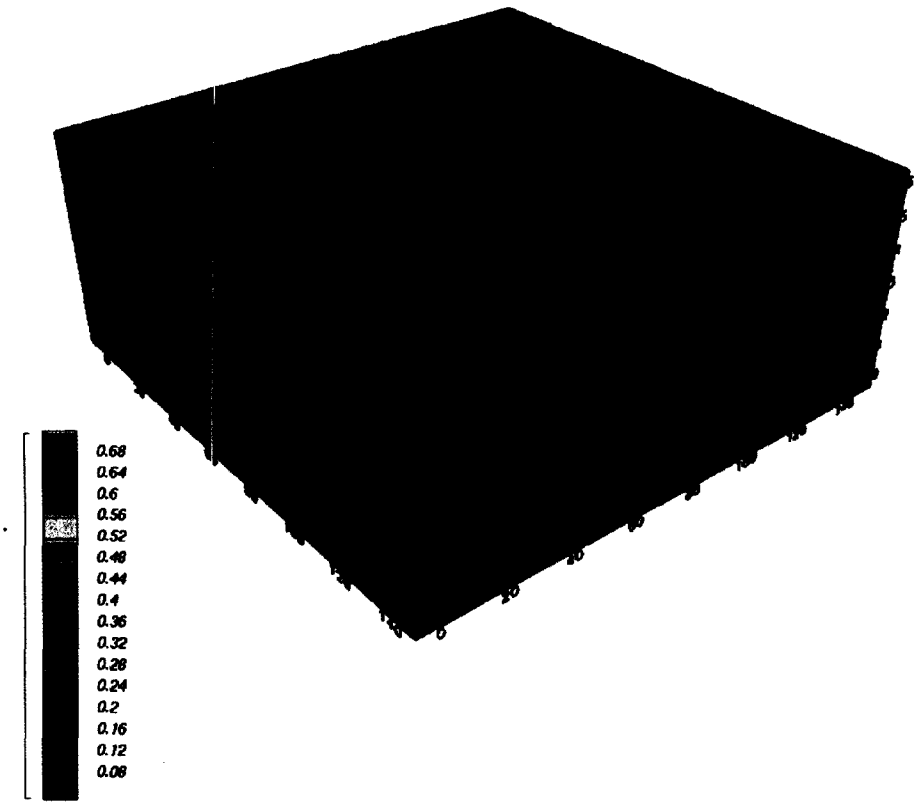

Fig. 10. Three-dimensional distributions of Newtonian oil at 20 years of waterflooding.

behind near the injection well for the Bingham oil case (Fig. 11), as compared with the Newtonian oil case (Fig. 10). All of these results explain that the waterflooding efficiency is poorer when dealing with a Bingham oil.

4.5 Summary of computational performance

Table 6 summarizes the numerical performance of the present model for the four sample problems. All the simulations were performed on a 100 MHz Pentium PC, and both direct and iterative solvers were used in these calculations. The convergence for nonlinear iterations was based on residual reduction to 1.0×10^{-5} or less relative to the accumulation terms for all the mass components at each grid block[24]. The automatic time-stepping scheme was used with a maximum time-step size specified for different problems. It is noted in the table that very small maximum time step size was used for problems 4.1 and 4.3, which is necessary to obtain sufficient accuracy in dealing with the Buckley–Leverett type displacement solving hyperbolic type equations.

5 CONCLUDING REMARKS

The primary objective of the present work was to present a numerical method to investigate transport phenomena of non-Newtonian fluids through porous media. Whenever non-Newtonian fluids are involved in porous media, the flow problem will become highly nonlinear because of the dependence of the apparent viscosity used in the Darcy equation on shear rate. In general a numerical method has to be resorted to analyze non-Newtonian fluid flow in porous media. In addition, the non-Newtonian flow behavior is quite different for different fluids and/or for different porous materials. Therefore it is impossible to develop a universal numerical approach for handling all flow problems involving various non-Newtonian fluids in porous media. In this work, major attention has been paid to developing a methodology for power-law and Bingham plastic fluids, since they are the most likely to be encountered in reservoirs. However, the proposed method should also be useful in analyzing flow problems of other types of non-Newtonian fluids.

A fully implicit three-dimensional integral finite difference model has been developed by modifying the general numerical codes, 'MULKOM/TOUGH2', to include the effects of non-Newtonian viscosity. This new simulator is capable of modeling both single and multiple phase non-Newtonian fluid flow through porous or fractured media. The numerical model can take account of all the important factors which affect the flow behavior of non-Newtonian and Newtonian fluids, such as capillary pressure,

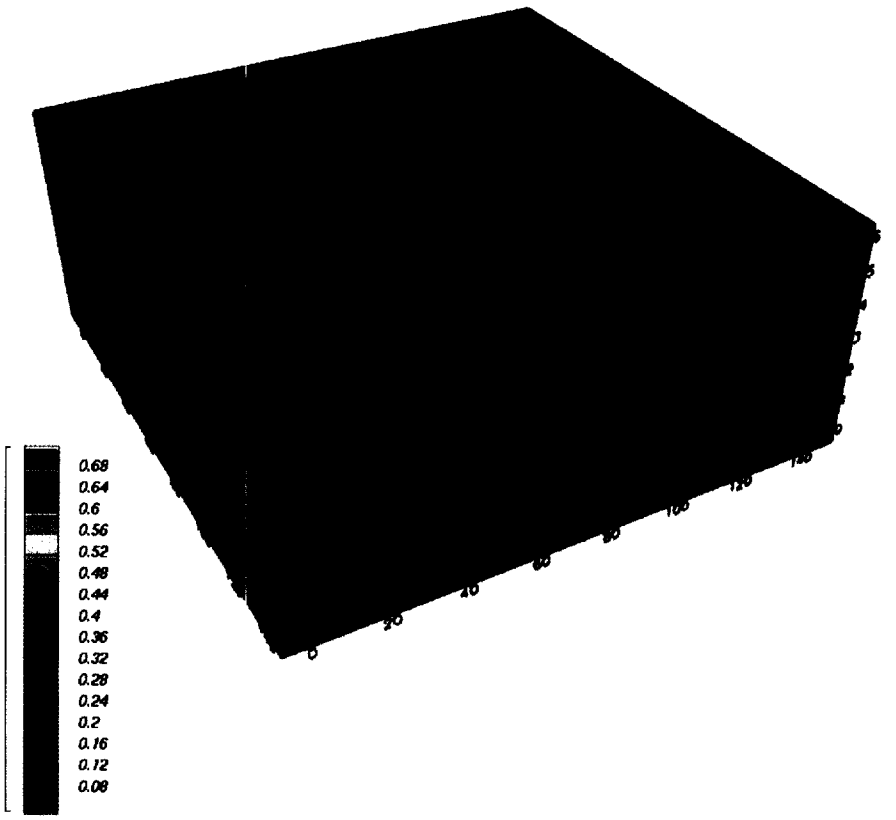

Fig. 11. Three-dimensional distributions of Bingham oil at 20 years of waterflooding.

complicated flow domains, in homogeneous porous and fractured media, and various well operation conditions. Several commonly used non-Newtonian rheological models have been incorporated in the code. The validity of the numerical method has been confirmed by comparing the model numerical results with analytical solutions for both single-phase and two-phase flow problems.

A three-dimensional, two-phase flow example is also presented to examine the model results using laboratory and simulation results existing for the three-dimensional problem with Newtonian fluid flow. A comparison between Newtonian and non-Newtonian displacement for the three-dimensional problem is discussed.

ACKNOWLEDGEMENTS

The authors are indebted to Chao Shan and Stefan Finsterle for their critical review of the manuscript. This work was supported in part through the Office of Environmental Management, the Office of Technology Development, and the US Department of Energy under contract no. DE-AC03-76SF00098. The authors are grateful to M. Fink, G. Chen and E. Karageorgi for their help in preparing the manuscript.

REFERENCES

1. Muskat, M., *The Flow of Homogeneous Fluids through Porous Media*. McGraw-Hill, New York, 1946.
2. Bear, J., *Dynamics of Fluids in Porous Media*. Elsevier, New York, 1972.
3. Scheidegger, A.E., *The Physics of Flow through Porous Media*. University of Toronto Press, 1974.
4. Savins, J.G. Non-Newtonian flow through porous media. *Industrial Engineering in Chemistry*, 1969, **61**(10) 18–47.
5. Wu, Y.-S., Theoretical studies of non-Newtonian and Newtonian fluid flow through porous media. Ph.D. Thesis, Earth Sciences Division, Lawrence Berkeley Laboratory, LBL-28642, University of California, Berkeley, CA, 1990.
6. Gogarty, W.B. Rheological properties of pseudo plastic fluids in porous media. *Society of the Petrol Engineering Journal*, 1967, **7** 149–159.
7. van Poollen, H.K. & Jargon, J.R. Steady-state and unsteady-state flow of non-Newtonian fluids through porous media. *Transactions of AIME*, 1969, **246** 80–88.
8. Odeh, A.S. & Yang, H.T. Flow of non-Newtonian power-law fluids through porous media. *Society of the Petrol Engineering Journal*, 1979, **19** 155–163.
9. Ikoku, C.U. & Ramey, H.J. Jr Transient flow of non-Newtonian power-law fluids in porous media. *Society of the Petrol Engineering Journal*, 1979, **19** 164–174.
10. McDonald, A.E., Approximate solutions for flow on non-Newtonian power-law fluids through porous media. Paper SPE 7690, presented at the SPE-AIME Fifth Symposium on Reservoir Simulation, Denver, CO, 1979.

11. Gencer, C.S. & Ikoku, C.U. Well test analysis for two-phase flow of non-Newtonian power-law and Newtonian fluids. *ASME Journal of Energy Resources Technology*, 1984, **106** 295–304.
12. Vongvuthipornchai, S. and Raghavan, R., Pressure falloff behavior in vertically fractured wells: non-Newtonian power-law fluids. SPE Formation Evaluation, 1987a, pp. 573–589.
13. Vongvuthipornchai, S. and Raghavan, R., Well test analysis of data dominated by storage and skin non-Newtonian power-law fluids. SPE Formation Evaluation, 1987b, pp. 618–628.
14. Buckley, S.E. & Leverett, M.C. Mechanism of fluid displacement in sands. *Transactions of AIME*, 1942, **146** 107–116.
15. Wu, Y.-S., Pruess, K. & Witherspoon, P.A. Displacement of a Newtonian fluid by a non-Newtonian fluid in a porous medium. *Transport in Porous Media*, 1991, **6** 115–142. (Report LBL-27412, Earth Sciences Division, Lawrence Berkeley Laboratory, CA).
16. Wu, Y.-S., Pruess, K. & Witherspoon, P.A. Flow and displacement of Bingham non-Newtonian fluids in porous media. *SPE Reservoir Engineering*, 1992, **0** 369–376.
17. Pruess, K. and Wu, Y.-S. On PVT-Data, Well treatment, and preparation of input data for an isothermal gas–water–foam version of MULKOM. Report LBL-25783, UC-403, Earth Sciences Division, Lawrence Berkeley Laboratory, Berkeley, CA, 1988.
18. Witherspoon, P.A., Benson, S., Persoff, P., Pruess, K., Radke, C.J. and Y.-S. Wu., Feasibility analysis and development of foam protected underground natural gas storage facilities. Final Report, Earth Sciences Division, Lawrence Berkeley Laboratory, CA, 1989.
19. Pruess, K. TOUGH2—a general-purpose numerical simulator for multiphase fluid and heat flow. Report LBL-29400, Earth Sciences Division, Lawrence Berkeley Laboratory, Berkeley, CA, 1991.
20. Gaucher, D.H. & Lindley, D.C. Water flood performance in a straitified, five-spot reservoir, a scaled model study. *Transactions of AIME*, 1960, **219** 208–215.
21. Coats, K.H., Neilsen, R.L., Terhune, M.H. & Weber, A.G. Simulation of three-dimensional two-phase flow in oil and gas reserviors. *Society of Petrol Engineering Journal*, 1967, **7** 377–388.
22. Wu, Y.S., Huyakorn, P.S. & Park, N.S. A vertical equilibrium model for assessing nonaqueous phase liquid contamination and remediation of groundwater systems. *Water Resources Research*, 1994, **30**(4) 903–912.
23. Pruess, K. Development of the general purpose simulator MULKOM. Annual Report, Earth Sciences Division, Lawrence Berkeley Laboratory, Berkeley CA, 1983.
24. Pruess, K. TOUGH User's Guide Report LBL-20700. Earth Sciences Division, Lawrence Berkeley Laboratory, Berkeley, CA, 1987.
25. Pruess, K. SHAFT, MULKOM, TOUGH—a set of numerical simulators for multiphase fluid and heat flow. Report LBL-24430, Earth Sciences Division, Lawrence Berkeley Laboratory, Berkeley, CA, 1988.
26. Narasimhan, T.N. & Witherspoon, P.A. An integrated finite difference method for analyzing fluid flow in porous media. *Water Resources Research*, 1976, **12**(1) 57–64.
27. Duff, I. S. MA28—a set of FORTRAN subroutines for sparse unsymmetric linear equations. AERE Harwell Report R 8730, 1977.
28. Moridis, G. and K. Pruess, T2CG1: a package of preconditional conjugate gradient solvers for the TOUGH2 family of codes. Report LBL-36235, Earth Sciences Division, Lawrence Berkeley Laboratory, Berkeley, CA, 1995.
29. Christopher, R.H. & Middleman, S. Power-law flow through a packed tube. *I and EC Fundamentals*, 1965, **4**(4) 422–426.
30. Wu, Y.S., Forsyth, P.A. & Jiang, H.A. A consistant approach for applying numerical boundary conditions for multiphase subsurface flow. *Journal of Contamination Hydrology*, 1996, **23** 157–184